Modulation of Aβ42 Aggregation Kinetics and Pathway by Low-Molecular-Weight Inhibitors

Marie-Theres Hutchison,[a] Giovanni Bellomo,[b] Alexey Cherepanov,[a] Elke Stirnal,[a] Boris Fürtig,[a] Christian Richter,[a] Verena Linhard,[a] Elina Gurewitsch,[a] Moreno Lelli,[c, f] Nina Morgner,[d] Thomas Schrader,[e] and Harald Schwalbe*[a]

The aggregation of amyloid-β 42 (Aβ42) is directly related to the pathogenesis of Alzheimer's disease. Here, we have investigated the early stages of the aggregation process, during which most of the cytotoxic species are formed. Aβ42 aggregation kinetics, characterized by the quantification of Aβ42 monomer consumption, were tracked by real-time solution NMR spectroscopy (RT-NMR) allowing the impact that low-molecular-weight (LMW) inhibitors and modulators exert on the aggregation process to be analysed. Distinct differences in the Aβ42 kinetic profiles were apparent and were further investigated kinetically and structurally by using thioflavin T (ThT) and transmission electron microscopy (TEM), respectively. LMW inhibitors were shown to have a differential impact on early-state aggregation. Insight provided here could direct future therapeutic design based on kinetic profiling of the process of fibril formation.

Introduction

Alzheimer's disease (AD) is the most common neurodegenerative disorder.[1] The pathogenesis of AD is complex, remains unclear and, to date, no cure exists.[2] Neuropathological indicators used to confirm AD include brain shrinkage, the presence of neurofibrillary tangles and amyloid plaques. These plaques are mainly comprised of the amyloid-β isoforms Aβ40 and Aβ42 with 40 or 42 amino acids, respectively. Aβ42 is the most pathogenic and aggregation-prone isoform.[3,4] Evidence from structural studies indicates differences between the fibrillar structures of the isoforms Aβ40 and Aβ42,[5–9] a mixed Aβ40/Aβ42 fibrillar species,[10] as well as different Aβ42 structures being observed.[11] The transient oligomeric species of Aβ40 has been observed to be more amorphous compared to Aβ42 that exhibits predominantly fibrillar structures.[12]

Current evidence strongly suggests that transient Aβ oligomers, formed during the initial stages of aggregation, and not the subsequent fibrils and plaques are responsible for neuronal cell death.[13] However, information directly relating to the initial stages of the aggregation process is scarce. The acceptance that early-stage oligomers are critical to pathogenesis has led to a change in strategies to intervene in the aggregating Aβ42 system.[14] Whereas previously treatments were aimed at preventing the formation of plaques or attempted to reverse and eliminate the plaques from systems affected by AD, many studies now focus on holding Aβ42 in monomeric form, as nontoxic oligomers, or on reversing oligomerization.[15,16]

This change of focus towards modulation of early-stage aggregation is mirrored also in the advances regarding aggregation models. Detailed models for Aβ42 and Aβ40 aggregation consider a two-species concept involving monomers and fibrils.[17,18] Further extensions of these models address secondary, surface-catalysed nucleation.[19,20] Yet, almost all of these studies test the proposed models against data which reflect on the formation of the fibrillar species alone.[17–21] Predominantly using thioflavin T (ThT) fluorescence data, monitoring formation of fibrillary species is the most widely adopted approach for investigating the aggregation kinetics.

An alternative for experimental quantification and modelling the aggregation process is to record data depicting monomer consumption,[23–26] including real-time monomer consumption information acquired by solution NMR spectroscopy.[27] Considering that several studies provided evidence that soluble oligomers convert to fibrillar structures,

[a] M.-T. Hutchison, Dr. A. Cherepanov, E. Stirnal, Dr. B. Fürtig, Dr. C. Richter, V. Linhard, E. Gurewitsch, Prof. Dr. H. Schwalbe
Institute for Organic Chemistry and Chemical Biology
Center for Biomolecular Magnetic Resonance (BMRZ)
Goethe University Frankfurt
Max-von-Laue-Str. 7, 60438 Frankfurt/Main (Germany)
E-mail: schwalbe@nmr.uni-frankfurt.de

[b] Dr. G. Bellomo
Laboratory of Clinical Neurochemistry
Department of Medicine and Surgery, University of Perugia
Piazzale Lucio Severi 1/8 06132 Perugia (Italy)

[c] Prof. Dr. M. Lelli
Chemistry Department, University of Florence
Via della Lastruccia 3, 50019 Sesto Fiorentino (Italy)

[d] Prof. Dr. N. Morgner
Institute for Physical and Theoretical Chemistry
Goethe University Frankfurt
Max-von-Laue-Str. 9, 60438 Frankfurt/Main (Germany)

[e] Prof. Dr. T. Schrader
Institute for Organic Chemistry, University of Duisburg-Essen
Universitätsstrasse 7, 45117 Essen (Germany)

[f] Prof. Dr. M. Lelli
Magnetic Resonance Center (CERM/CIRMMP)
University of Florence
Via Luigi Sacconi 6, 50019 Sesto Fiorentino (Italy)

ChemBioChem

Research Article
doi.org/10.1002/cbic.202200760

Chemistry
Europe
European Chemical
Societies Publishing

these transient species also deserve inclusion into kinetic models.[28,29]

In 2018, Bellomo et al. recorded experimental NMR data quantifying monomer consumption which was modelled by describing the formation of transient oligomers, the conversion of oligomers into fibrils, and the polymerization of fibrils by the association of oligomers. The oligomer-to-fibril-conversion step was shown to require a critical size that depends on monomer concentration. Furthermore, the study demonstrated that ThT and solution NMR data are consistent.[30] Recently, Michaels et al. found that most oligomers dissociate to monomers instead of forming fibrils. Higher monomer concentrations resulted in faster fibrillization. In addition, the model was used to predict the effect of Brichos, a molecular chaperone and inhibitor of secondary nucleation, on aggregation in terms of oligomer concentration against aggregation time.[31]

Subsequently, a kinetic investigation, with a primary focus on the oligomer diversity of several aggregating systems, identified two major commonalities for oligomers. Presence of oligomers dissociating back to monomeric species, instead of maturing directly into fibrillar entities, is a common feature found in all investigated aggregating systems, which indicates that these oligomers are nonfibrillar. Based upon this kinetic model, the oligomer behaviour is related to oligomer persistence, convertibility and abundance.[32] In another very recent paper, the authors investigated the formation of transient Aβ42 species, with a particular focus on secondary nucleation, by solution NMR, ThT and cryo-EM, coupled with simulations.[33] Real-time solution NMR revealed an Aβ42 aggregation profile with a double-sigmoidal curve and an intermediate plateau in between. ThT fluorescence data exhibited an intensity decrease which occurs at the same time as the plateau observed by NMR spectroscopy. Furthermore, the inhibitor chaperone Brichos was employed to investigate the connection between the presence of the intermediates and secondary nucleation.[33]

Here, we report the characterization of the effect of different low-molecular-weight inhibitors on the complex aggregation process of Aβ42. In particular, we investigated the effect of molecular tweezers CLR01 and CLR03 as well as peptides OR1 and OR2 (chemical structures are shown in Figure 1) on Aβ42 aggregation. CLR01 is a supramolecular tweezer that can bind to lysine and arginine residues of peptide and proteins with 10 and 30 micromolar affinities, respectively.[34] It binds to R5, K16 and K28 in Aβ40 and Aβ42. In-depth studies on the effect of CLR01 complexation on the assembly process of Aβ have previously been published.[35] In previous NMR studies, Aβ40 was investigated due to its slower aggregation kinetics. A recent LILBID-MS and ESI investigation has led to a new model of self-assembly in early-state aggregation which distinguishes between two critical dimer conformations in Aβ (Figure S21 in the Supporting Information), one of which leads to rapid aggregation into toxic species. The impact of CLR01 and OR2 on the self-assembly process of Aβ42 was further investigated and revealed the inhibitory effect of CLR01 to be comparable to that of OR2. Both, CLR01 and OR2 were found to inhibit dimer-base (DB) dimer formation.[36] Inhibition of β-sheet formation and fibril formation in the Aβ samples, incubated with CLR01,
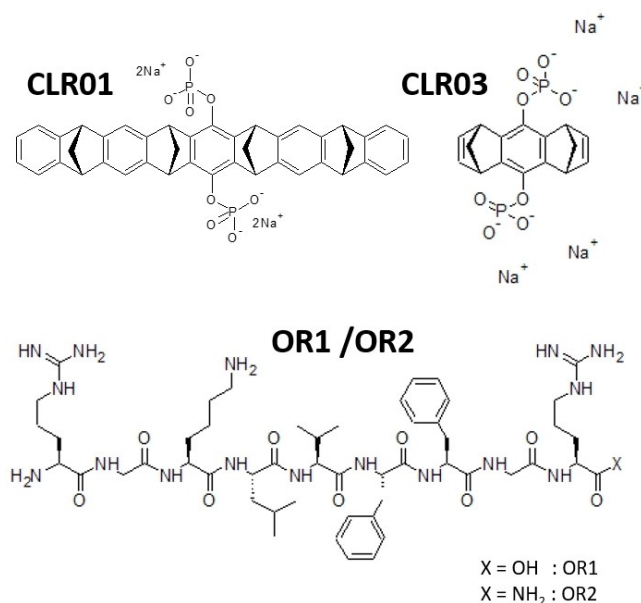

Figure 1. Low-molecular-weight inhibitors and modulators of Aβ aggregation. CLR01, a molecular tweezer specific for lysine and arginine, includes the side chains of basic amino acid residues inside its hydrophobic cavity. CLR03 is the negative control without a cavity. OR1 and OR2 are both RGKLVFFGR peptides based on the core hydrophobic region of Aβ, KLVFF, with OR1 carrying a C-terminal carboxylic acid and OR2 the respective amide.

was reported. Where oligomerization was identified, the nature of the species appeared to become more amorphous in the presence of CLR01. Importantly, a CLR01-induced reduction in the toxic effects exerted by Aβ in neuronal cells as well as in transgenic mice was demonstrated.[37]

Here, we compare the effect of the CLR01-interaction with that of three additional low-molecular-weight Aβ42 aggregation modulators including the KLVFF peptides OR1 and OR2, and CLR03, the truncated control of CLR01. In contrast to CLR01, no inhibition of Aβ β-sheet formation was observed upon CLR03 addition, which lacks the hydrophobic walls and thus serves as negative control. We focused our analysis on real-time solution NMR data from the early-stage aggregation of Aβ42 by tracking monomer consumption, in the presence and absence of these inhibitors and modulators.

Comparison of the influence of different inhibitors and modulators on aggregation kinetics is technically demanding, as batch-to-batch reproducibility has to be assured. We show batch-to-batch reproducibility for the aggregation kinetics of Aβ42 alone and find consistent data for the concentration dependence of Aβ42 aggregation kinetics. To this end, we have conducted the kinetic experiments consistently at Aβ concentrations of 90 and 100 μM (batch specific concentrations) and at a temperature of 293 K. Additional ThT and TEM experiments supplemented our experimental NMR aggregation kinetics to yield further information on aggregation kinetics and fibril morphology.

Results and Discussion

We characterized the interaction of CLR01, of CLR03, and of the KLVFF peptides OR1 and OR2 to Aβ42 by solution NMR spectroscopy. The initial 2D [^{1}H,^{15}N] HSQC spectrum of Aβ42 at 278.5 K showed low peak dispersion characteristic of an intrinsically disordered protein and overlayed well with previously published spectra of monomeric Aβ42, from which the backbone assignment of residues could be transferred. The spectra of Aβ42 in the absence of aggregation modulators exhibited a uniform loss of signal intensity over time, without observable line broadening of NMR correlation peaks during the time course of the aggregation process.

The interaction of the inhibitors with freshly prepared samples of ^{15}N-labelled Aβ42 was monitored in [^{1}H,^{15}N] HSQC spectra in sodium phosphate buffer, pH 7.2, 278.5 K (Figures S6–9 and S12–15). Changes in Aβ42 resonances could be identified at a concentration of 6 μM CLR01 to 60 μM Aβ42, similar to previous reports for Aβ40.[15] Upon addition of CLR01, a non-uniform loss of signal intensity of the resonances was apparent (Figures S6–S9). The most significant change occurred in the regions around two lysine residues, K16 and K28. At saturating CLR01, the residues E3, A2/30, I31/V24, G9, G38, V39, V40, I41 and A42 were least affected (Figure S7). Residues perturbed upon addition of substoichiometric amounts of CLR01 to Aβ42 overlapped with those affected in the Aβ40 isoform.[15]

In order to consider the contribution of the hydrophobic arms of CLR01 to its interaction mode, we conducted titration experiments with CLR03 (Figure S12) which lacks this feature, but still possesses the phosphate groups. In contrast to previously published data wherein no perturbations were observed at [Aβ40]/[CLR03] = 1:4, we observed small CSPs (Figure S12).

Several studies have shown the important role peptidomimetics can play in altering the course of aggregation pathways. We therefore also investigated the interaction of the KLVFF peptides OR1 and OR2 with Aβ42. Residues exhibiting pronounced CSPs were found in the region H13-L17 for [Aβ42]/[peptide] = 1:4. In addition, CSPs at K28 and R5, with complete loss of signal intensity at N27, and in the case of OR2 also H14 were observed. Taken together, the CSPs and signal intensity loss NMR data after the addition of CLR01, CLR03, OR1 and OR2 to Aβ42 indicate that most of the interaction occurs with residues bearing positive side-chains. Furthermore, the interaction occurs primarily with the pre-central hydrophobic core residues H13–L17, as well as region around K28, and to a lesser extent the region around R5.

Subsequently, we investigated how these molecules affect the aggregation process by real-time solution NMR, compared the experimental kinetics, and evaluated it accordingly. It is known that several factors influence the aggregation kinetics of Aβ42, including concentration, pH, ionic strength and temperature.[30] To investigate interactions and monitor aggregation kinetics, we kept the pH to physiological 7.2. 1D ^{1}H NMR information was used to monitor kinetics as opposed to HSQC spectral information as this offered better signal-to-noise ratio and high temporal resolution, allowing for a more detailed overview of the aggregation process.

In the Aβ40 profiles shown in the work of Bellomo et al.,[30] a lag phase was observed at concentrations ranging from 30 μM via 50 μM to 100 μM. This lag phase was followed by a fast decay of the monomer signal until no further signal decrease was observed.

In our experiments, the 1D ^{1}H spectra of the methyl region of Aβ42 showed a decrease in signal intensity without associated line broadening or shifts in the monomeric Aβ42 signals during the aggregation process (Figure 2a). We analysed a well-resolved signal in the methyl region at 0.63 ppm to track monomer loss over time. Residual signals under the methyl region 0.7–0.85 ppm may represent flexible parts of fibrils.[39–41] For Aβ42 in the absence of inhibitors (Figure 2b, Aβ only profile), the kinetic data do not exhibit an initial lag phase. Contrary to what has been observed in Bellomo et al. for Aβ40,[30] a fast exponential decay is observed within the first six hours of starting the kinetics and over 70% of the starting signal intensity is lost. Thereafter, an increase (ca. 5%) in monomer signal becomes apparent. The remaining signal intensity then undergoes a second moderate to slow decay until it levels out and no further signal loss is observed. The NMR experiments were repeated three times at a starting concentration of 100 μM Aβ42 and showed highly reproducible kinetic profiles of monomer depletion. Notably, the slight increase in the monomer signal was consistently observed in the three acquired profiles. In comparison to the general sigmoidal kinetic profiles reported for Aβ40 and Aβ42 prior to our investigation, the Aβ42 kinetic profile indicated distinct differences.[30] These differences may be due to the heightened aggregation propensity of Aβ42 versus Aβ40, the higher concentration of Aβ42 used in our studies, or that the aggregation pathway of Aβ42 is different to that of Aβ40. Recently, similar kinetic trends as observed here have been reported for Aβ42.[33]

We next investigated the influence of LMW inhibitors and modulators on the kinetic profile of Aβ42. Based on the 2D HSQC data, CLR01, CLR03, OR1 and OR2 all appeared to interact at the same sites of unfolded monomeric Aβ42, primarily with residues bearing positive side-chains, at the pre-central hydrophobic core as well as around K28 and R5 (Figure S15). However, a basic shape analysis of the aggregation traces for OR1, OR2, CLR01 and CLR03 show distinctly different profiles for all inhibitors (Figure 2b).

The kinetic traces for Aβ42 alone and with CLR01 both started with an initial fast exponential signal decrease. The presence of CLR01 suppressed the increase in monomer signal observed in the kinetic profile for Aβ42 alone. By contrast, in terms of different phases of the decreasing monomer signal, the profile of Aβ42-CLR03 resembles more closely that of Aβ42 alone than Aβ42 with CLR01. Aβ42-OR1 and Aβ42-OR2 kinetic profiles are similar. Kinetics of Aβ42 aggregation in the presence of OR2 is characterized by a single exponential intensity decrease. For OR1, a similar exponential decrease is seen as for Aβ42-OR2. However, after ca. 67 hours, the signal begins to decrease further. It is also clear from the analysis of
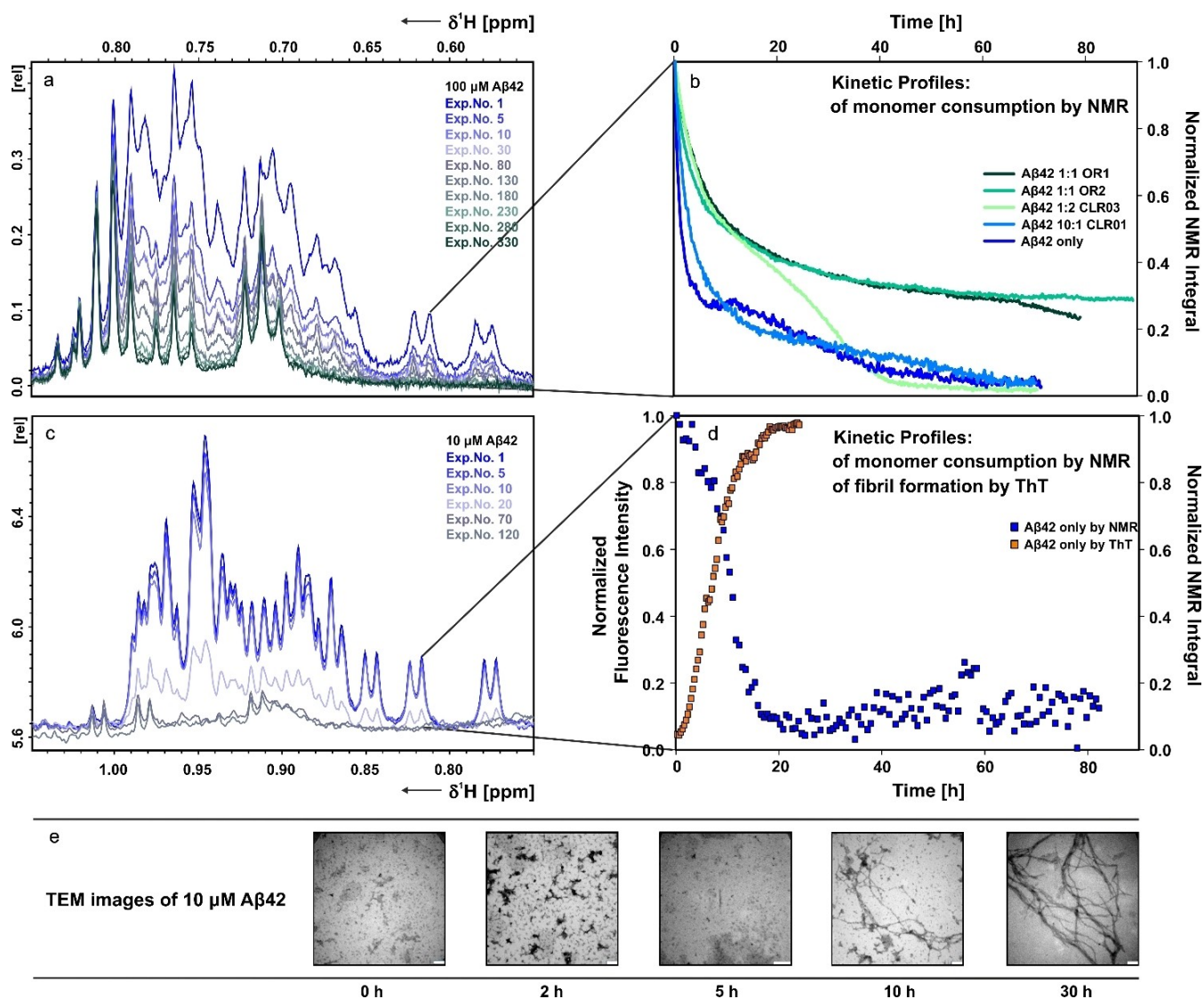
ChemBioChem

Research Article
doi.org/10.1002/cbic.202200760

Chemistry Europe
European Chemical
Societies Publishing

Figure 2. Aβ42 aggregation kinetics are altered by the presence of LMW modulators and inhibitors. a) Overlay of 1D ^{1}H NMR spectra of the methyl signals of 100 μM Aβ42 at pH 7.2 and 293 K over a 65-h time course. The well resolved methyl signal at 0.61 ppm was used as a reporter signal, as potential signal contributions from flexible fibril regions can be seen under signals from 0.70–0.85 ppm, and the methyl signal at 0.58 ppm overlaps with that of OR1 and OR2. b) Monomer consumption kinetic profiles of Aβ42 alone, 10 Aβ42: 1 CLR01, 1 Aβ42: 2 CLR03, 1 Aβ42: 1 OR2, and 1 Aβ42: 1 OR1. The ratios chosen were based on the minimum concentrations required to exert indicators of interaction in terms of CSPs and peak intensity change in the initial 2D [^{1}H,^{15}N] HSQC interaction study. For Aβ42 alone and 10 Aβ42: 1 CLR01, a starting concentration of 100 μM was used, and for 1 Aβ42: 2 CLR03, 1 Aβ42: 1 OR2, and 1 Aβ42: 1 OR1 the starting concentration was 90 μM Aβ42. The spectra were recorded at 700 MHz and 293 K, in 15 mM sodium phosphate, 55 mM NaCl, pH 7.2, 10% D$_2$O. NMR kinetic spectral data were plotted by using Dynamic Centre. c) Overlay of 1D ^{1}H NMR spectra of the methyl signals of 10 μM Aβ42 at pH 7.2 and 310 K over an 82-h time course. The well resolved methyl signal at 0.82 ppm was used as a reporter signal for aggregation kinetics. The spectra were recorded at 950 MHz and 310 K in 15 mM sodium phosphate, 55 mM NaCl, pH 7.2, 10% D$_2$O. d) Monomer consumption kinetics of 10 μM Aβ42 by 1D ^{1}H NMR overlaid with fibril formation kinetics of 10 μM Aβ42 monitored by changes of ThT fluorescence at 310 K. The kinetic profile shows normalized 1D ^{1}H NMR methyl signals of 10 μM Aβ42 versus time, with no obvious lag phase (blue squares). The changes in the normalized ThT fluorescence intensity of Aβ42 alone vs time were recorded for 24 h (orange squares). For clarity, each orange square represents an average of 10 datapoints. The ThT fluorescence of 10 μM Aβ42 was recorded at 310 K at 120 s intervals under quiescent conditions, and the solution was not shaken, to mimic NMR conditions. (Further ThT fluorescence information, depicting all individual datapoints, on Aβ42 fibril formation in the presence of small molecule inhibitors and modulators is presented in Figures S19 and 3a). e) TEM images of Aβ42 samples withdrawn at reaction start, 0 h, and during the aggregation time course 2, 5, 10, and 30 h after the start of the reaction. The reaction conditions were 10 μM Aβ42 at pH 7.2 and 310 K in 15 mM sodium phosphate, 55 mM NaCl, pH 7.2, 10% D$_2$O under quiescent conditions; scale bars: 0.1 μm. (Further structural information regarding 10 μM Aβ42 in the presence of small-molecule inhibitors and modulators by TEM during the aggregation time course is shown in Figures S22–S26.)

these profiles that the signal intensity does not drop below 20%, whereas all other depicted modulator profiles drop close to 0% residual intensity.

In order to confirm the presence of fibrillar species upon completion of the NMR kinetics, NMR samples were diluted and transmission electron microscopy (TEM) images were acquired. TEM showed Aβ42 fibrils to be present in the absence of any

ChemBioChem

Research Article
doi.org/10.1002/cbic.202200760

Chemistry
Europe
European Chemical
Societies Publishing

modulators. However, upon addition of CLR01 to the preformed fibrils, globular, amorphous structures could be identified. This correlates with previous information reporting CLR01 capable of altering preformed aggregates (Figure 3).

As both ThT and TEM experiments are routinely performed at concentrations lower than those used to perform the NMR interaction studies and RT-NMR kinetics, RT-NMR kinetics of monomer consumption were repeated with initial conditions of 10 μM monomeric Aβ42, at pH 7.2 and 310 K. Also, at the lower concentration of 10 μM we do not observe a pronounced initial lag phase. We observe a decrease, followed by a transient dip in monomer signal at approximately 7 hours, and a continued decrease in signal that reaches a final plateau (Figure 2d).

Due to the structurally promiscuous nature of Aβ42, it was important to determine whether the formation of on-pathway fibrils occurred under the conditions used to record the NMR kinetics. Thus, ThT fluorescence change and TEM studies were performed. The ThT kinetics performed for 10 μM monomeric Aβ42, pH 7.2 and 310 K, exhibit no prolonged lag phase, a signal increase until about 7 h, at which a temporary halt and slight signal decrease is visible. The signal thereafter continues to increase until it reaches a final plateau in approximately 20 h (Figure 4a The ThT kinetics for Aβ42 with OR1 (Figure 4d) resemble those of Aβ42 with CLR03 (Figure 4c) for the first 24 h. The kinetic profile of Aβ42 with CLR01 deviates from all other traces. In stark contrast to the other profiles, the ThT signal initially decreases, possesses a lag phase that lasts approximately 15 hours whereafter the signal increases steeply until about 30 h after which the signal increase is slower until the ultimate plateau is reached at around 40 h (Figure 4b).

Fitting of the ThT kinetics was performed using the online, open-access platform Amylofit.[22] The traces were processed for
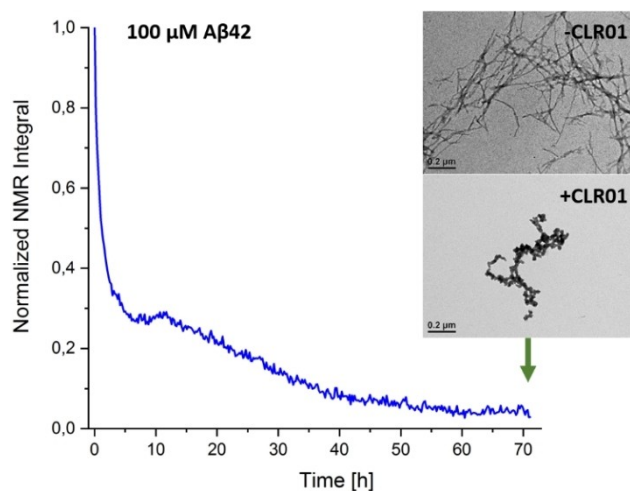
baseline and endpoint plateau corrections and normalized to a scale of 0–1. The models: nucleation elongation, fragmentation dominated, fragmentation and secondary nucleation, saturating elongation, saturating elongation and elongation, saturating elongation and fragmentation and the corresponding unseeded version of these models all fail to achieve a reasonable fit of the Aβ42: CLR01 kinetics. The models: secondary nucleation dominated, and multistep secondary nucleation dominated, and the corresponding unseeded versions of these models best fit the Aβ42: CLR01 experimental ThT kinetics, as well as achieving a suitable fit for Aβ42 alone, Aβ42: CLR03 and Aβ42: OR1 (Figures S27–S30). These models report on differences with respect to the rate changes observed for primary nucleation, elongation and secondary nucleation. Regarding comparison of kinetic profiles, a shift only in aggregation initiation along the time axis without curve shape change reflects inhibition of primary nucleation. No shift in the start of aggregation initiation, coupled with a prolonged time in which the same amplitude is reached indicates an inhibition of secondary nucleation. An inhibition of elongation is characterised by a sigmoidal curve which exhibits an extended initializing step followed by a slower increase in signal until a plateau is reached.[19]

Comparing the experimental kinetic ThT profiles, we observe relatively minor deviations between Aβ42 alone, Aβ42: CLR03 and Aβ42: OR1. In contrast, the Aβ42: CLR01 profile shows a delay in the start of ThT fluorescence change by approximately 17 h which correlates to an inhibition of primary nucleation. This is reflected in the relative combined rate constant k_+k_n of Aβ42: CLR01 versus Aβ42 alone which is significantly decreased in comparison to Aβ42: CLR03 and Aβ42: OR1 versus Aβ42 only.

A decrease in the rates k_+ and k_+k_n for Aβ42: CLR01 versus Aβ42 alone is seen in both the fitting of the ThT data and the fitting of NMR kinetic data according to the conversion model (10 μM and 100 μM Aβ42 start concentration, respectively; Tables 1 and S1–S11). Relative rate changes for all processes are not compared as the ThT and NMR model fittings each focus on certain processes. For example, secondary nucleation rate information is not compared for the ThT and NMR fitting between the models as the (NMR) conversion model places a focus on oligomer growth and conversion of oligomers to fibrils whereas the model for ThT fitting focuses on secondary nucleation as a process.

TEM was used to further cross validate our RT-NMR kinetics data (Figures S22–S26). We withdrew samples (from independent reactions) for TEM analysis at set time points of 0, 2, 5, 10 and 30 h in the absence and presence of CLR01, OR1 and CLR03. No fibrillar structures were apparent in TEM images

Figure 3. 1D ¹H NMR aggregation kinetics of Aβ42, and TEM images depicting on-pathway fibrils at the conclusion of the kinetics and for CLR01-treated amorphous Aβ42. The experimental NMR kinetic profile according to the intensity decrease in the monomer signal from the methyl region of 1D ¹H NMR experiments recorded at 700 MHz is presented in the absence of any modulator. The Aβ42 starting concentration was 100 μM, at pH 7.2 and 293 K. TEM shows on-pathway fibrils for Aβ42 after completion of kinetics; upon addition of CLR01, amorphous aggregates are observed.

Table 1. Relative combined rate constants. An increased rate is shown in burgundy and decreased rate in blue.		
Secondary nucleation dominated, unseeded	k_+k_n	k_+k_n
(Aβ42＋CLR01)/Aβ42	4.81×10^{-5}	1.96
(Aβ42＋CLR03)/Aβ42	2.58	9.61×10^{-10}
(Aβ42＋OR1)/Aβ42	2.69	0.123

ChemBioChem

Research Article
doi.org/10.1002/cbic.202200760

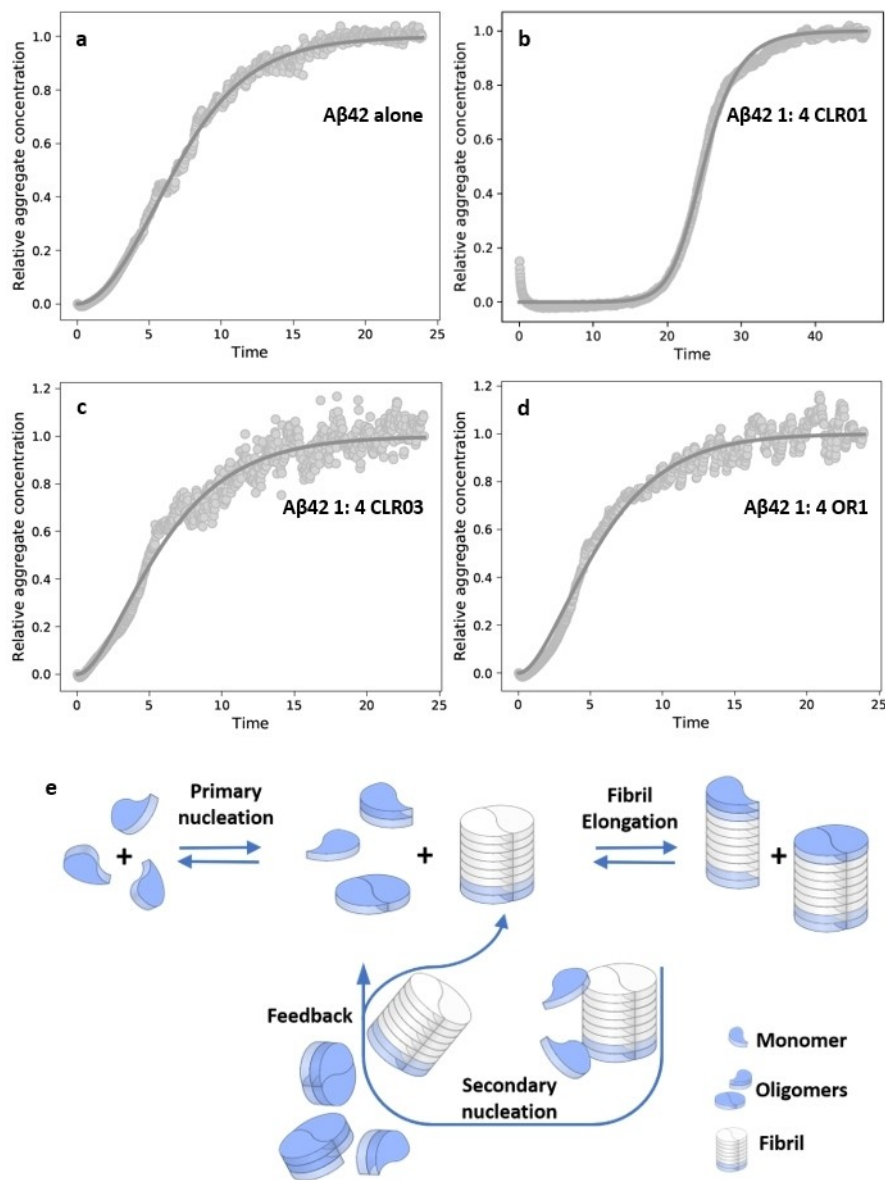**Chemistry Europe**
European Chemical
Societies Publishing

Figure 4. Fitting Aβ42 aggregation kinetics in the absence and presence of LMW inhibitors and modulators. The aggregation kinetics of 10 μM Aβ42 were monitored through the change in ThT fluorescence in a) the absence and presence of 40 μM b) CLR01, c) CLR03 and d) OR1. ThT kinetics were recorded at 310 K and pH 7.2 in 15 mM sodium phosphate, 55 mM NaCl, pH 7.2, 10% D_2O, at 120 s intervals under quiescent conditions. Experimental datapoints are depicted as circles and the corresponding fit as a solid line. The model, secondary nucleation dominated, unseeded, applied in the above fitting of Aβ42 in the absence or presence of CLR01, CLR03 and OR1 reports on k_n: the primary nucleation constant, k_+: the elongation rate constant, and k_2: the secondary nucleation rate constant, by generating the combined rate constants k_+k_n and k_+k_2. The reaction orders for primary and secondary nucleation, n_c and n_2, were set to 2. (For further model fitting information see Figures S27–S31 and Tables S1–S11. TEM images of Aβ42 in the absence and presence of CLR01, CLR03 and OR1 at reaction start, $t=0$ h, and $t=2, 5, 10$ and 30 h are depicted in Figures S22–S26, respectively). e) Schematic representation of Aβ42 amyloid aggregation as described by the model used to fit the ThT aggregation kinetics. Primary nucleation, elongation, and secondary nucleation processes are considered in this model, and the impact of inhibitors and modulators on aggregation kinetics is observed in terms of the rates in which these steps occur.

taken at 0 h. Small dots could, however, be seen which may already depict loose interactions for Aβ42 alone. Furthermore, at $t=0$ h, we also see occasional larger round structures that may represent Aβ42 in micellular structures. The $t=2$ h TEM images reveal what appears to be the growth of not well-defined fibrillar structures often with local depletion of the dots and occasional close localization to the potential micelles. In these images, again no well-defined, mature fibrils can be seen. At $t=30$ h, well-defined fibrillar structures can be seen in all

samples except for Aβ42 in the presence of CLR01, where seldom fibrils were found, and those found looked structurally instable.

Conclusion

We have monitored real-time monomeric Aβ42 aggregation kinetics by solution NMR spectroscopy and have compared

information regarding the formation and behaviour of various aggregating species. We provide insight into what effects four different low-molecular-weight modulators exert during the early stages of the aggregation process. Our investigation demonstrates that LMW modulators and inhibitors are generally able to interact with the same regions and residues of Aβ42, but that their complexation results in different modulation of the aggregation kinetics. Analysis of the aggregation kinetic profiles by solution NMR spectroscopy illustrates different phases in monomer signal intensity loss. Based on a qualitative comparison of the kinetic profiles, the addition of CLR01 influences Aβ42 aggregation; in particular, the transient plateau observed for Aβ42 alone is absent in the presence of CLR01. As Aβ42: CLR01 oligomer growth preferentially occurs in a monomer-based (MB) stacking fashion, resulting in amorphous and potentially less-toxic species, it could be speculated that a shift towards the MB growth scheme might contribute to this difference in kinetic profile.

Interestingly, we consistently observed a transient increase in monomer concentration during the course of Aβ42 aggregation without modulators. To validate these kinetic findings, we recorded TEM images to investigate Aβ42 fibril morphology. Initially at $t = 0$ h, no significant proportion of fibrils or larger structures wsd observed, except for Aβ42 in the presence of CLR01 where amorphous rather than fibrillar structures were observed. At $t = 2$ h, TEM images for all samples, except Aβ42 with CLR01, exhibited smaller fibril growths and micellular structures. Both the smaller fibril growths and micellular structures dissipated throughout the course of aggregation ($t = 5, 10$ h) to be replaced initially by immature, rather branched, growing fibrils, and finally by mature fibrils at $t = 30$ h. We propose that the growing fibril might reject Aβ monomers due to a favourable oligomer-monomer interaction in terms of dimer-base growth (Figure S21), and that this growth scheme may be illustrated by the branched growth seen at $t = 10$ h and could be a factor contributing to the sedimentation observed in previous studies. In addition, it could explain why Aβ42 with CLR01, which favours a MB-fibril growth, does not exhibit a double sigmoidal in the kinetics.

Further, based on the model fitting of Aβ42 ThT aggregation kinetics in the absence and presence of CLR01, OR1 and CLR03, it would appear that CLR01 predominantly interacts by decreasing the rate of primary nucleation and elongation, and only shows a slight increase in the rate of secondary nucleation and elongation. In contrast, both CLR03 and OR1 increase the rate of primary nucleation and elongation, and decrease the rate of secondary nucleation and elongation with respect to Aβ42 alone.

Our work contributes towards extending our knowledge of the more pathogenic isoform, Aβ42, and gaining a more complete understanding of the kinetics of the amyloidogenic process as a whole. This in turn might uncover a structure-activity relationship for different inhibitors or modulators of pathologic protein aggregation. A profound kinetic understanding of Aβ aggregation could therefore help rationalize therapeutic efforts to alleviate the toxic nature of AD and modulate disease progression.

Conflict of Interest

The authors declare no conflict of interest.

Data Availability Statement

The data that support the findings of this study are available in the supplementary material of this article.

[1] Alzheimer's Association Report, "*Alzheimer's Dement.* **2020**, *16*, 391–460.
[2] D. J. Selkoe, J. Hardy, *EMBO Mol. Med.* **2016**, *8*, 595–608.
[3] G. G. Glenner, C. W. Wong, *Biochem. Biophys. Res. Commun.* **1984**, *120*, 885–890.
[4] J. Davis-Salinas, S. M. Saporito-Irwin, C. W. Cotman, W. E. Van Nostrand, *J. Neurochem.* **1995**, *65*, 931–934.
[5] I. Bertini, L. Gonnelli, C. Luchinat, J. Mao, A. Nesi, *J. Am. Chem. Soc.* **2011**, *133*, 16013–16022.
[6] J. X. Lu, W. Qiang, W. M. Yau, C. D. Schwieters, S. C. Meredith, R. Tycko, *Cell.* **2013**, *154*, 1257.
[7] Y. Xiao, B. Ma, D. McElheny, S. Parthasarathy, F. Long, M. Hoshi, R. Nussinov, Y. Ishii, *Nat. Struct. Mol. Biol.* **2015**, *22*, 499–505.
[8] M. A. Wälti, F. Ravotti, H. Arai, C. G. Glabe, J. S. Wall, A. Böckmann, P. Güntert, B. H. Meier, R. Riek, *Proc. Natl. Acad. Sci. USA* **2016**, *113*, 4976–4984.
[9] M. T. Colvin, R. Silvers, Q. Z. Ni, T. V. Can, I. Sergeyev, M. Rosay, K. J. Donovan, B. Michael, J. Wall, S. Linse, R. G. Griffin, *J. Am. Chem. Soc.* **2016**, *138*, 9663–9674.
[10] L. Cerofolini, E. Ravera, S. Bologna, T. Wiglenda, A. Böddrich, B. Purfürst, I. Benilova, M. Korsak, G. Gallo, D. Rizzo, L. Gonnelli, M. Fragai, B. De Strooper, E. E. Wanker, C. Luchinat, *Chem. Commun.* **2020**, *56*, 8830–8833.
[11] Y. Yang, D. Arseni, W. Zhang, M. Huang, S. Lövestam, M. Schweighauser, A. Kotecha, A. G. Murzin, S. Y. Peak-Chew, J. Macdonald, I. Lavenir, H. J. Garringer, E. Gelpi, K. L. Newell, G. G. Kovacs, R. Vidal, B. Ghetti, B. Ryskeldi-Falcon, S. H. W. Scheres, M. Goedert, *Science* **2022**, *375*, 167–172.
[12] N. J. Economou, M. J. Giammona, T. D. Do, X. Zheng, D. B. Teplow, S. K. Buratto, M. T. Bowers, *J. Am. Chem. Soc.* **2016**, *138*, 1772–1775.
[13] D. M. Walsh, I. Klyubin, J. V. Fadeeva, W. K. Cullen, R. Anwyl, M. S. Wolfe, M. J. Rowan, D. J. Selkoe, *Nature* **2002**, *416*, 535–539.
[14] J. Hardy, *J. Neurochem.* **2009**, *110*, 1129–1134.
[15] S. Sinha, D. H. Lopes, Z. Du, E. S. Pang, A. Shanmugam, A. Lomakin, P. Talbiersky, A. Tennstaedt, K. McDaniel, R. Bakshi, P. Y. Kuo, M. Ehrmann, G. B. Benedek, J. A. Loo, F. G. Klärner, T. Schrader, C. Wang, G. Bitan, *J. Am. Chem. Soc.* **2011**, *133*, 16958–16969.
[16] J. L. Chang, A. J. Hinrich, B. Roman, M. Norrbom, F. Rigo, R. A. Marr, E. M. Norstrom, M. L. Hastings, *Mol. Ther.* **2018**, *26*, 1539–1551.
[17] S. I. A. Cohen, M. Vendruscolo, M. E. Welland, C. M. Dobson, E. M. Terentjev, T. P. J. Knowles, *J. Chem. Phys.* **2011**, *135*, 1–44.
[18] G. Meisl, X. Yang, E. Hellstrand, B. Frohm, J. B. Kirkegaard, S. I. A. Cohen, C. M. Dobson, S. Linse, T. P. Knowles, *Proc. Natl. Acad. Sci. USA* **2014**, *111*, 9384–9389.

ChemBioChem

Research Article
doi.org/10.1002/cbic.202200760

Chemistry
Europe
European Chemical
Societies Publishing

[19] S. Linse, *Biophys. Rev. Lett.* **2017**, *9*, 329–338.

[20] S. I. A. Cohen, S. Linse, L. M. Luheshi, E. Hellstrand, D. A. White, L. Rajah, D. E. Otzen, M. Vendruscolo, C. M. Dobson, T. P. Knowles, *Proc. Natl. Acad. Sci. USA.* **2013**, *110*, 9758–9763.

[21] I. Bertini, G. Gallo, M. Korsak, C. Luchinat, J. Mao, E. Ravera, *ChemBioChem* **2013**, *14*, 1891–1897.

[22] G. Meisl, J. B. Kirkegaard, P. Arosio, T. C. Michaels, M. Vendruscolo, C. M. Dobson, S. Linse, T. P. Knowles, *Nat. Protoc.* **2016**, *11*, 252–272.

[23] C. Gerum, R. Silvers, J. Wirmer-Bartoschek, H. Schwalbe, *Angew. Chem. Int. Ed.* **2009**, *48*, 9452–9456; *Angew. Chem.* **2009**, *121*, 9616–9620.

[24] C. Gerum, K. Schlepckow, H. Schwalbe, *J. Mol. Biol.* **2010**, *401*, 7–12.

[25] J. Kumar, S. Sreeramulu, T. L. Schmidt, C. Richter, J. Vonck, A. Heckel, C. Glaubitz, H. Schwalbe, *ChemBioChem* **2010**, *11*, 1208–1213.

[26] K. Schlepckow, H. Schwalbe, *Angew. Chem. Int. Ed.* **2013**, *52*, 10002–5; *Angew. Chem.* **2013**, *125*, 10186–10189.

[27] N. L. Fawzi, J. Ying, D. A. Torchia, G. M. Clore, *J. Am. Chem. Soc.* **2010**, *132*, 9948–9951.

[28] M. Ahmed, J. Davis, D. Aucoin, T. Sato, S. Ahuja, S. Aimoto, J. I. Elliott, W. E. Van Nostrand, S. O. Smith, *Nat. Struct. Mol. Biol.* **2010**, *17*, 561–567.

[29] J. Lee, E. K. Culyba, E. T. Powers, J. W. Kelly, *Nat. Chem. Biol.* **2011**, *7*, 602–609.

[30] G. Bellomo, S. Bologna, L. Gonnelli, E. Ravera, M. Fragai, M. Lelli, C. Luchinat, *Chem. Commun.* **2018**, *54*, 7601–7604.

[31] T. C. T. Michaels, A. Šarić, S. Curk, K. Bernfur, P. Arosio, G. Meisl, A. J. Dear, S. I. A. Cohen, C. M. Dobson, M. Vendruscolo, S. Linse, T. P. J. Knowles, *Nat. Chem.* **2020**, *12*, 445–451.

[32] A. J. Dear, T. C. T. Michaels, G. Meisl, D. Klenerman, S. Wu, S. Perrett, S. Linse, C. M. Dobson, T. P. J. Knowles, *Proc. Natl. Acad. Sci. USA* **2020**, *117*, 28–31.

[33] M. Törnquist, R. Cukalevski, U. Weininger, G. Meisl, T. P. J. Knowles, T. Leiding, A. Malmendal, M. Akke, S. Linse, *Proc. Natl. Acad. Sci. USA.* **2020**, *117*, 1–9.

[34] M. Fokkens, T. Schrader, F. G. Klärner, *J. Am. Chem. Soc.* **2005**, *127*, 14415–14421.

[35] S. Sinha, Z. Du, P. Maiti, F. G. Klärner, T. Schrader, C. Wang, G. Bitan, *ACS Chem. Neurosci.* **2012**, *3*, 451–458.

[36] T. Lieblein, R. Zangl, J. Martin, J. Hoffmann, M. Hutchison, T. Stark, E. Stirnal, T. Schrader, H. Schwalbe, N. Morgner, *eLife* **2020**, *9*, 1–30.

[37] A. Attar, C. Ripoli, E. Riccardi, P. Maiti, D. D. Li Puma, T. Liu, J. Hayes, M. R. Jones, K. Lichti-Kaiser, F. Yang, G. D. Gale, C. H. Tseng, M. Tan, C. W. Xie, J. L. Straudinger, F. G. Klärner, T. Schrader, S. A. Frautschy, C. Grassi, G. Bitan, *Brain* **2012**, *135*, 3735–3748.

[38] B. Barz, A. K. Buell, S. Nath, *Chem. Commun.* **2021**, *57*, 947.

[39] I. Matlahov, P. C. A. van der Wel, *Methods* **2018**, *148*, 123–135.

[40] J. Wang, T. Yamamoto, J. Bai, S. J. Cox, K. J. Korshavn, M. Monette, A. Ramamoorthy, *Chem. Commun.* **2018**, *54*, 2000–3.

[41] H. Heise, W. Hoyer, S. Becker, O. C. Andronesi, D. Riedel, M. Baldus, *Proc. Natl. Acad. Sci. USA* **2005**, *102*, 15871–15876.